Available online at www.sciencedirect.com
SCIENCE DIRECT®
Biomaterials 25 (2004) 1141–1150
Biomaterials
www.elsevier.com/locate/biomaterials

Dental composites based on hybrid and surface-modified amorphous calcium phosphates

D. Skrtic[a,*], J.M. Antonucci[b], E.D. Eanes[b], N. Eidelman[a]

[a] American Dental Association Foundation, Paffenbarger Research Center, National Institute of Standards and Technology, 100 Bureau Drive Stop 8546, Gaithersburg, MD 20899, USA

[b] Polymers Division, National Institute of Standards and Technology, Gaithersburg, MD 20899, USA

Received 11 July 2003; accepted 7 August 2003

Abstract

The objectives of this study were to prepare hybrid and surface-modified amorphous calcium phosphates (ACPs) as fillers for mineral-releasing dental composites, and determine whether the mechanical strength of the composites could be improved without decreasing their remineralization potential. ACP was hybridized with tetraethoxysilane or zirconyl chloride and surface-treated with 3-methacryloxypropoxytrimethoxy silane (MPTMS) or zirconyl dimethacrylate (ZrDMA). Composites fabricated with unmodified ACP (u-ACP), hybrid or surface-modified ACP filler and photo-activated Bis-GMA, TEGDMA and 2-hydroxyethyl methacrylate (HEMA) (BTH resin), Bis-GMA, TEGDMA, HEMA and MPTMS (BTHS resin) or Bis-GMA, TEGDMA, HEMA and ZrDMA (BTHZ resin) were tested for their remineralizing potential and biaxial flexure strength (BFS). Ion releases from all composites were significantly above the minimum necessary for reprecipitation of apatite. The BFS of unfilled polymers was not adversely affected by immersion in saline solutions. The BFS of BTH and BTHS composites deteriorated upon soaking. However, BTHZ composites were practically unaffected by exposure to saline solutions. Filler hybridization resulted in a modest, but significant, improvement in the BFS (up to 24%) of BTHZ composites. Heterogeneous distribution of the ACP on disk surfaces was detected by the FTIR microspectroscopy analyses. This might have been caused by uncontrolled aggregation of ACP particles that appeared to hinder interfacial filler/resin interactions and diminish the mechanical strength of composites.

Keywords: Amorphous phosphate; Dental restorative material; Mechanical strength; FTIR microspectroscopy

1. Introduction

In the early 1990s we developed a bioactive mineral-ion-releasing composite based on a polymer matrix phase derived from ambient polymerization of acrylic monomers and a filler phase consisting of amorphous calcium phosphate (ACP). When the ACP was stabilized by pyrophosphate ($P_2O_7^{4-}$) ions ($P_2O_7^{4-}$ retards conversion of ACP to apatite (Ap)), it was possible to take advantage of ACP's relatively high solubility and obtain substantial release of Ca^{2+} and PO_4 ions [1]. Moreover, the levels attained from these releases were sustainable [2] and could promote the recovery of mineral deficiencies in tooth structures in vitro [3]. However, $P_2O_7^{4-}$-stabilized ACP-filled composites are relatively weak because ACP does not act as reinforcing filler in a manner similar to that of commonly used silanized glass fillers. The introduction of silica or zirconia into stabilized ACP fillers by low temperature sol–gel techniques is a possible route to synthesize hybrid ACP fillers with improved reinforcing ability and mechanical strength without adversely affecting their mineral ion-release capability. Additionally, surface treatment of the fillers [4] with organofunctional silanes and/or zirconyl methacrylate should enhance chemical ACP/matrix bonding without weakening the interface in a composite formulation.

The goals of this study were to assess the feasibility of synthesizing hybrid and surface-modified ACPs, and to evaluate whether treatments with hybridizing and/or surface-modifying agents actually improve the mechanical strength of the composites without impeding their remineralizing potential.

In addition to previously described procedures for evaluating the efficacy of various treatments [5],

*Corresponding author. Tel.: +1-301-975-3541; fax: +1-301-963-9143.
E-mail address: drago.skrtic@nist.gov (D. Skrtic).

0142-9612/$ - see front matter © 2003 Elsevier Ltd. All rights reserved.
doi:10.1016/j.biomaterials.2003.08.001

physicochemical characterization of the composites was done by utilizing Fourier-Transform Infrared microspectroscopy in reflectance mode (FTIR-RM), a non-contact, non-destructive method capable of characterizing both qualitatively and quantitatively the chemical properties of the surface of optically thick polymer specimens [6]. FTIR-RM mapping, previously used to determine the actual distribution of the different chemical components in human gallstones [7] and the minerals in pisoliths [8] and dentin [9], was explored as a tool for identifying inorganic functional groups of ACP fillers and the organic components of the resin in the composite specimens.

2. Materials and methods

2.1. Resin formulations

The matrix resins were formulated from commercially available dental monomers and photo-initiators used for visible-light polymerization (Table 1). Resins designated as BTH (Bis-GMA, TEGDMA and 2-hydroxyethyl methacrylate (HEMA)), BTHS (Bis-GMA, TEGDMA, HEMA and MPTMS) and BTHZ (Bis-GMA, TEGDMA, HEMA and ZrDMA) were photo-activated by inclusion of camphorquinone (CQ) and ethyl-4-*N,N*-dimethylaminobenzoate (4EDMAB) as the photo-oxidant and photo-reductant, respectively (Table 2). The chemical structures of the monomers, coupling agents and components of the photo-initiating system are given in Fig. 1.

2.2. Synthesis of the ACP fillers

ACP fillers were synthesized employing the protocol of Eanes et al. [10]. P_2O_7 stabilized ACP was precipitated instantaneously in a closed system (under CO_2-free N_2 in order to minimize CO_2 adsorption by the precipitate) at 22°C upon rapidly mixing equal volumes

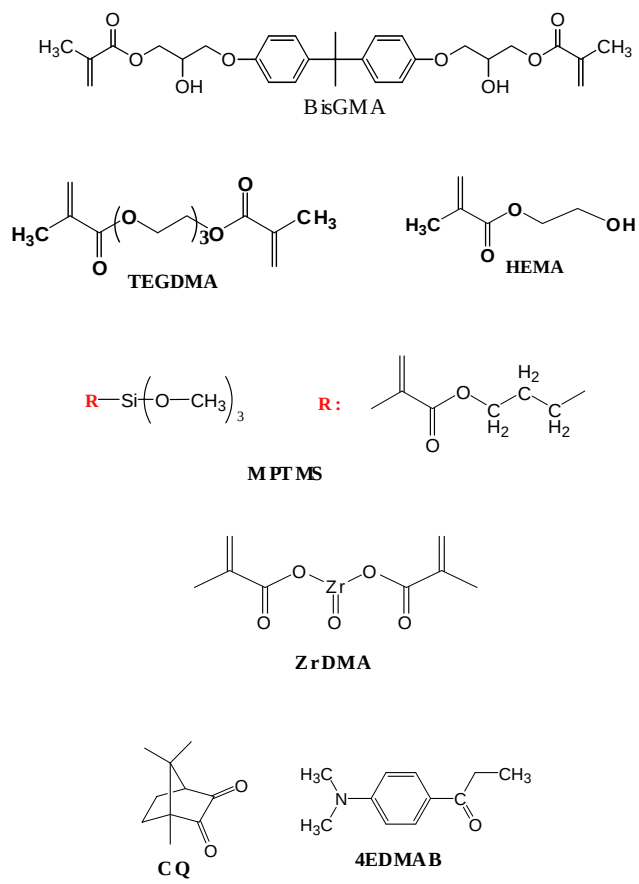

Fig. 1. Chemical structures of the monomers, coupling agents and the components of the photo-initiating system used to formulate the resins.

Table 1

Acronyms, chemical names and sources of monomers and photo-initiator system components employed for resin formulations

Acronym	Name	Manufacturer
Bis-GMA	2,2-Bis[*p*-(2′-hydroxy-3′-methacryloxypropoxy)phenyl]-propane	Freeman Chemical Corp., Port Washington, WI
TEGDMA	Triethyleneglycol dimethacrylate	Esstech, Essington, PA
HEMA	2-Hydroxyethyl methacrylate	Esstech, Essington, PA
MPTMS	3-Methacryloxypropoxytrimethoxy silane	Aldrich Chem. Co., Milwaukee, WI
ZrDMA	Zirconyl dimethacrylate	Rohm Tech. Inc., Malden, MA
CQ	Camphorquinone	Aldrich Chem. Co., Milwaukee, WI
4EDMAB	Ethyl-4-*N,N*-dimethylamino benzoate	Aldrich Chem. Co., Milwaukee, WI

Table 2
Composition of photo-activated resins (mass fraction, %)

Component/resin	Bis-GMA	TEGDMA	HEMA	MPTMS	ZrDMA	CQ	4EDMAB
BTH	35.5	35.5	28.0	—	—	0.2	0.8
BTHS	30.5	30.5	18.0	10.0	—	0.2	0.8
BTHZ	35.5	35.5	27.0	—	1.0	0.2	0.8

of a 800 mmol/l $Ca(NO_3)_2$ solution and a 536 mmol/l Na_2HPO_4 solution that contained a molar fraction of 2% $Na_4P_2O_7$. The reaction pH was between 10.5 and 11.0. This ACP is designated as unmodified ACP (u-ACP).

Tetraethoxysilane (TEOS)- and zirconyl chloride ($ZrOCl_2$)-hybridized ACPs (Si- and Zr-ACP, respectively) were prepared by simultaneously adding appropriate volumes of the $Ca(NO_3)_2$ solution and either a previously prepared TEOS solution (mass fraction of 10% TEOS, 10% ethanol, 10% tartaric acid and 70% water) or a 0.25 mol/l $ZrOCl_2$ solution to the Na_2HPO_4 solution. The TEOS solution was designed to prevent premature gelation of TEOS [4]. The respective volumes of the hybridizing solutions used were adjusted to achieve molar ratios of $ZrOCl_2$:Na_2HPO_4 and TEOS:Na_2HPO_4 equal to 0.1. The reaction pH was between 9.0–9.3 and 8.6–9.0 for the preparation of Si- and Zr-ACP, respectively. The suspensions were filtered, and the solid phase was washed with ice-cold ammoniated water and lyophilized.

2.3. Surface treatment of ACP fillers

Si- and Zr-ACP powders were each surface treated with 3-methacryloxypropoxytrimethoxy silane (MPTMS; mass fraction of 10% based on the amount of ACP [4]) or zirconyl dimethacrylate (ZrDMA; mass fraction of 1% based on the amount of ACP [11]). Si- or Zr-ACP powder was silanized with MPTMS as follows: MPTMS was mixed into a slurry of ACP powder in cyclohexane containing a mass fraction of 2% *n*-propylamine (based on the amount of ACP). The MPTMS-ACP/cyclohexane/*n*-propylamine mixture was rotary evaporated (100°C; moderate vacuum: 2.7 kPa) to remove the solvents, cooled to room temperature (23°C), washed with cyclohexane to remove residual MPTMS and unattached products, and re-dried under vacuum. ZrDMA was applied to Zr-ACP powder in a similar fashion with methylene chloride being used as the solvent.

2.4. Characterization of the ACP fillers

The ACP powders used as fillers in this study (Table 3) were characterized by powder X-ray diffraction (XRD) and Fourier-transform infrared spectroscopy (FTIR). The XRD patterns of the powdered samples were recorded in the 4–60° 2θ range with Cu$K\alpha$ radiation ($\lambda = 0.154$ nm) using a Rigaku 2200 D-Max X-ray diffractometer (Rigaku/USA Inc., Danvers, MA, USA) operating at 40 kV and 40 mA. The samples were step-scanned in intervals of 0.010° 2θ at a scanning speed of 1.0°/min. The same scanning conditions were also applied in examining composite disk specimens for the extent of internal ACP to Ap conversion upon exposure to aqueous environments.

The FTIR spectra (4000–400 cm^{-1}) of the filler powders suspended in KBr pellets were recorded using a Nicolet Magna-IR FTIR 550 spectrophotometer (Nicolet Instrument Corporation, Madison, WI, USA). KBr pellets were made of approximately 2 mg of the powder and 400 mg of KBr.

The particle size distribution (PSD) of the ACP fillers was determined by using a centrifugal particle size analyzer (model SA-CP3, Shimadzu Scientific Instruments, Inc., Columbia, MD, USA). ACP powder was dispersed in isopropanol and utrasonicated for 10 min at room temperature prior to the analysis (triplicate runs for each experimental group). The median particle size diameter (d_m) and the corresponding specific surface area (SSA) of the sample were obtained from the PSD data.

Thermal decomposition profiles of the ACP fillers were recorded by using a Perkin-Elmer 7 Series Thermal Analysis System (Perkin-Elmer, Norwalk, CT, USA). Five to 10 milligrams of powdered ACP samples were heated at the rate of 20°C/min (30–600°C temperature range) in an N_2 atmosphere. The overall water content (mass fraction, %) and a relative ratio of surface-bound/structural water were calculated from the thermogravimetric data.

The Ca/PO_4 ratios of the solids after dissolution in HCl were calculated from the corresponding solution Ca^{2+} and total PO_4 concentration values. Ca^{2+} was

Table 3
Composition, structure and size of ACP fillers used in the study

Filler	Hybridizing agent	Surface modifier	Ca/PO_4 mole ratio[a]	Water content[b] (mass %)	Median diameter[c] (μm)	SSA[c] (mm^2/g)
u-ACP	None	None	1.50±0.09	11.86±2.36	6.01±1.50	0.64±0.15
Si-ACP	TEOS	None	1.59±0.06	12.82±2.00	8.85±1.84	0.37±0.17
Zr-ACP	$ZrOCl_2$	None	1.91±0.09	17.28±1.59	7.41±2.27	0.54±0.27
Si/Si-ACP	TEOS	MPTMS	1.47±0.11	13.75±1.05	5.79±1.56	0.61±0.25
Zr/Zr-ACP	$ZrOCl_2$	ZrDMA	2.19±0.07	14.32±1.79	7.44±1.50	0.39±0.08

[a] Ca/PO_4 values given as the mean±standard deviation. Number of repetitive experiments in each group $n \geqslant 5$.
[b] Results of the thermogravimetric analysis. Reported values represent mean±standard deviation for three or more samples in each group.
[c] Results of the PSD analysis expressed as mean±standard deviation. Number of runs in each group $n \geqslant 5$.

determined by atomic absorption spectroscopy (AAS) with a Perkin-Elmer Model 603 spectrophotometer (Perkin-Elmer, Norwalk, CT, USA) using an air-acetylene flame and the 422.7 nm wavelength line. Ca^{2+} standards were prepared from weighed amounts ($\pm$0.1% mass fraction) of NIST Standard Reference Material $CaCO_3$ (dried at 250°C for 2 h). Both standard Ca solutions and the unknown samples contained 1000 mg kg^{-1} $LaCl_3$. PO_4 was determined by UV/VIS spectroscopy as a blue molybdato complex in acidified ammonium molybdate solution containing ascorbic acid and a small amount of antimony [12] using a Carey Model 219 spectrophotometer (Varian Analytical Instruments, Palo Alto, CA, USA) at a wavelength of 882 nm. The PO_4 standards were prepared from weighed amounts ($\pm$0.1% mass fraction) of KH_2PO_4 (dried at 105°C for 2 h). Absorbances of both standards and unknowns were determined at essentially the same aging time (approximately 1 h) by observing color development in the sample cell versus an H_2O blank.

Surface morphology/topology of ACP powders was determined by scanning electron microscopy (SEM) using a JEOL, JSM-5400 instrument (JEOL, Japan).

2.5. Preparation and characterization of composite disk specimens

Composite pastes were made from various resins (Table 2; mass fraction 60%) and ACP fillers (Table 3; mass fraction 40%) and were mixed by hand spatulation. The homogenized pastes were kept under moderate vacuum (2.7 kPa) overnight to eliminate the air entrained during mixing. The pastes were then molded in disks (15.8–19.8 mm in diameter and 1.55–1.81 mm in thickness) by filling the circular openings of flat teflon molds, covering each side of the mold with a mylar film plus a glass slide, and then clamping the assembly together with spring clips. The disks were photopolymerized by irradiating each face of the mold assembly for 120 s with visible light (Triad 2000, Dentsply International, York, PA, USA). After post-curing at 37°C in air for 24 h, the intact disks were directly examined by XRD.

2.6. Mineral ion release from the composites

The dissolution/transformation behavior of the composite specimens was examined at 37°C in HEPES-buffered (pH = 7.40) 240 mOsm/kg saline solutions. Each individual disk specimen was suspended by means of a stainless steel wire frame in 100 ml of continuously stirred test solution. Ion release kinetics was followed by taking aliquots at appropriate time intervals, filtering (Millex GS filter assemblies; Millipore, Bedford, MA, USA) and measuring the solution Ca^{2+} and PO_4 concentrations. Upon completion of the immersion tests (240 h or longer), the disks were removed, dried, and examined by XRD and/or FTIR-RM. Three or more separate immersion runs were performed for each experimental group. Kinetic ion-release data was corrected for variations in the total area of the disk surface exposed to the immersion solution. Exposed disk areas ranged from 450 to 690 mm^2, with the majority of the values clustered around 500 mm^2. Therefore, the filtrate Ca^{2+} and PO_4 values were normalized to 500 mm^2 using the simple relation for a given surface area, A: normalized value = (measured value) $\times$ (500/A).

2.7. Mechanical strength of the composites

Biaxial flexure strength (BFS) of dry and wet (after at least 240 h of immersion in buffered saline solution) composite disk specimens was determined by using a computer-controlled Universal Testing Machine (Instron 5500R, Instron Corp., Canton, MA) operated by Instron Merlin Software Series 9. The failure stress was calculated according to the following equation [13,14]:

$$\mathrm{BFS} = AL/t^2, \quad (1)$$

where $A = -[3/4\pi(X-Y)]$, $X = (1+\nu)\ln(r_l/r_s)^2 + [(1-\nu)/2](r_l/r_s)^2$, $Y = (1+\nu)[1+\ln(r_{sc}/r_s)^2]$, ν is the Poisson's ratio, r_l the radius of the piston applying the load at the surface of contact, r_{sc} the radius of the support circle, r_s the radius of disk specimen, L the applied load at failure, and t the thickness of disk specimen.

2.8. FTIR microspectroscopy (FTIR-RM)

The FTIR-RM measurements were performed by using a Nicolet Magna-IR™ 550 FTIR spectrophotometer interfaced with a Nic-Plan IR microscope operated in reflectance mode. The microscope was equipped with a video camera to display images, with a liquid nitrogen cooled-mercury cadmium telluride (MCT) detector (Nicolet Instrumentations Inc., Madison, WI, USA) and with a computer-controlled mapping stage, programmable in the x and y directions (Spectra-Tech, Inc., Shelton, CT, USA).

Whole and fractured segments of the composite disk specimens were placed on KBr windows or mounted and leveled in holders, and then placed on the motorized stage. The spectral point-by-point mapping of the surface of the specimens was done in a grid pattern with the use of the computer-controlled microscope stage and Omnic® Atlus™ Microscope software in reflectance mode. The FTIR reflectance spectra were rationed against the background of a gold-coated disk. The specimens were initially focused in the middle of their surfaces and then mapped automatically in the 700–4000 cm^{-1} region with 8 cm^{-1} resolution, aperture of 200 $\times$ 200 μm, steps of 200–400 μm and 64 scans per spectrum (except the spectra of the cross section of the

Si-ACP/BTH disk that were scanned 512 times each). The mapped specimens were kept in exact same position on the motorized stage until all areas of interest were examined with individual focus and with various sizes of apertures and number of scans. The FTIR maps were processed as individual phosphate (PO_4) and carbonyl (CO) profiles (PO_4 from filler and CO from resin components) and displayed usually as color contour distribution maps next to the corresponding visual surface maps of the specimens. In order to better compare the representative reflectance spectra from the full specimens maps and/or from individually focused points with more commonly used absorbance spectra, reflectance spectra were transformed to "absorbance-like" spectra by using the dispersion correction (Kramers-Kronig transform algorithm) [6,15] available in the Omnic software.

2.9. Data analysis

Experimental data were analyzed by multi-factorial ANOVA ($\alpha = 0.05$). Pairwise multiple comparison procedures were performed to determine significant differences between specific groups. One standard deviation was given in this paper for comparative purposes as the estimated standard uncertainty of the measurements. These values should not be compared with data obtained in other laboratories under different conditions.

3. Results

A typical FTIR spectrum and XRD pattern of the ACP fillers used in this study are shown in Fig. 2a and b. There was no significant difference in structural features of unmodified, hybridized and/or surface modified ACPs. The amorphous character of the ACPs is evidenced by two very broad peaks in the XRD patterns. Corresponding FTIR spectra generally showed two wide bands typical of ACP, i.e. ν_1 and ν_3 PO_4 stretching (1200–900 cm^{-1}) and ν_4 PO_4 bending (630–500 cm^{-1}).

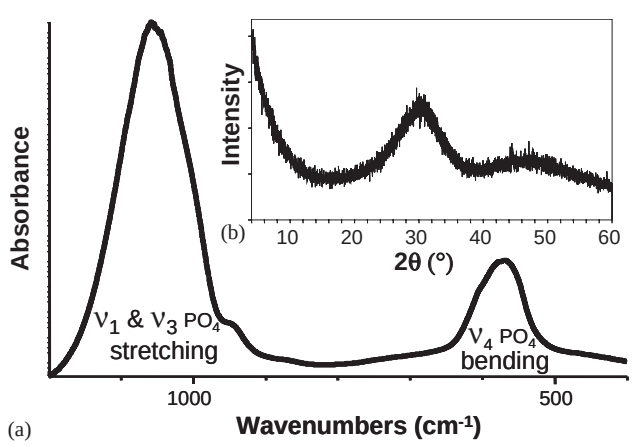

Fig. 2. A typical FTIR spectrum (a) and XRD pattern (b) of the ACP fillers used in the study.

SEM microphotographs of u-ACP, Si-ACP, Zr-ACP, Si/Si-ACP and Zr/Zr-ACP powders are presented in Fig. 3a–e. Particles of both hybridized (Fig. 3b and c) and surface-treated ACPs (Fig. 3d and e) showed no evident textural/morphological difference compared to u-ACP (Fig. 3a). The Ca/PO_4 molar ratio of u-ACP, Si-ACP and Si/Si-ACP powders also showed no significant differences (Table 3). This ratio was, however, significantly higher for all Zr-treated ACPs, with the Zr/Zr-ACP having the highest value (2.19; $p<0.05$, two-tail test). While the u-ACP, Si-ACP and Si/Si-ACP powders dissolved completely in HCl (a step that was performed for the analyses of Ca and PO_4), all of the Zr-ACP and Zr/Zr-ACP were not fully dissolved. The FTIR spectra of these HCl-insoluble solids indicated the presence of PO_4 groups that were different from the PO_4 groups of the ACPs that dissolved completely in HCl. These PO_4 absorptions might have originated from small amounts of Zr-PO_4 compounds that precipitated during the Zr-ACP and Zr/Zr-ACP synthesis. All the ACPs had heterogeneous PSDs with particle diameters ranging from 0.1 to 80 μm. Apparent differences in the median diameters and the SSA of the fillers (columns 6 and 7 in Table 3, respectively) were found statistically insignificant (two-tailed Tukey test). Total water content of the fillers ranged from a mass fraction of 11.86% to a mass fraction of 17.28% (column 5, Table 3). All pairwise comparisons indicated that the amount of incorporated water was significantly higher in Zr-ACP compared to the other types of fillers.

The release, upon soaking, of remineralizing Ca^{2+} and PO_4 ions into the surrounding aqueous media was affected by both resin composition and the type of the ACP filler utilized (Table 4). u-ACP/BTH, u-ACP/BTHS, u-ACP/BTHZ, Si-ACP/BTH, Si-ACP/BTHZ and Zr-ACP/BTHZ composites exhibited the highest ion release. Significantly lower ion release ($p<0.05$; Tukey-test) was observed in Si-ACP/BTHS, Zr-ACP/BTH and all composites that utilized surface treated fillers. Nevertheless, the aqueous levels of Ca^{2+} and PO_4 ions reached in these systems were significantly above the minimum needed for remineralization to occur, i.e. all solutions were supersaturated with respect to Ap [16].

The results of the BFS screening (Table 5) showed that the strength of unfilled BTH, BTHS and BTHZ resin disks was not adversely affected by immersion. The BFS of unfilled BTH specimens was higher than the BFS of BTHS or BTHZ specimens (i.e., the resins containing MPTMS or ZrMA, respectively). Filled BTH and BTHS composites, regardless of the type of ACP filler utilized, showed significant deterioration in their strength upon soaking. Among filled composites only those based on

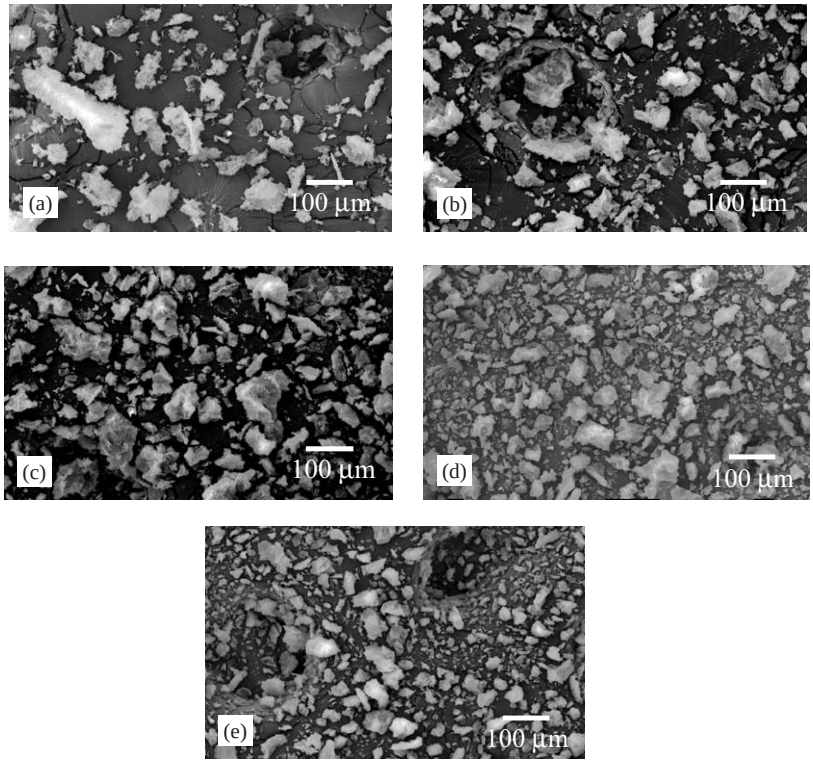

Fig. 3. SEM microphotographs of (a) u-ACP, (b) Si-ACP, (c) Zr-ACP, (d) Si/Si-ACP and (e) Zr/Zr-ACP powders.

Table 4
The maximum levels of Ca^{2+} and PO_4 ions released upon soaking various composite disk specimen in buffered (pH = 7.40) saline solution at 37°C (time interval 240 h)

Filler	BTH		BTHS		BTHZ	
	Ca (mmol/l)	PO_4 (mmol/l)	Ca (mmol/l)	PO_4 (mmol/l)	Ca (mmol/l)	PO_4 (mmol/l)
u-ACP	1.03 (0.10)	0.65 (0.09)	1.06 (0.12)	0.62(0.07)	0.93 (0.09)	0.59 (0.02)
Si-ACP	0.96 (0.09)	0.63 (0.06)	0.74 (0.11)	0.48 (0.02)	0.99 (0.11)	0.64 (0.05)
Zr-ACP	0.58 (0.05)	0.36 (0.02)	—	—	0.99 (0.08)	0.63 (0.06)
Si/Si-ACP	0.66 (0.06)	0.43 (0.02)	0.58 (0.03)	0.38 (0.02)	—	—
Zr/Zr-ACP	0.62 (0.03)	0.37 (0.01)	—	—	0.57 (0.03)	0.35 (0.01)

Results represent mean values with standard deviations given in parenthesis. Number of runs in each experimental group ⩾ 3.

Table 5
Biaxial flexure strength (BFS) of dry and wet composite disk specimens tested before and after immersion in buffered saline solutions, respectively

Filler	BTH		BTHS		BTHZ	
	BFS (MPa)		BFS (MPa)		BFS (MPa)	
	Dry	Wet	Dry	Wet	Dry	Wet
None	243 (39)	177 (59)	126 (17)	148 (31)	110 (23)	132 (35)
u-ACP	70 (8)	44 (8)	62 (2)	40 (3)	59 (7)	55 (11)
Si-ACP	60 (12)	26 (14)	49 (5)	42 (12)	73 (9)	67 (14)
Zr-ACP	43 (11)	37 (6)	—	—	67 (8)	66 (11)
Si/Si-ACP	61 (13)	48 (19)	51 (8)	39 (6)	—	—
Zr/Zr-ACP	72 (7)	39 (4)	—	—	77 (9)	51 (5)

Results represent mean values with standard deviations given in parenthesis. Number of runs in each experimental group ⩾ 3.

BTHZ resin (with exemption of wet Zr/Zr-ACP/BTHZ) were essentially unaffected by exposure to saline solutions. A modest (between 14% and 24%), but statistically significant ($p < 0.05$; Tukey test), improvement in the BFS of BTHZ composites was observed when u-ACP was substituted with hybrid ACP. Surface

modified ACP fillers (except in dry Zr/Zr-ACP BTHZ composites), however, did not improve the BFS of the composites. Both the XRD patterns and the FTIR spectra of ground post-immersion samples showed almost none or only a minimal conversion of hybrid and/or surface modified ACP fillers to Ap. By contrast, composites filled with u-ACP exhibited a significant conversion to Ap under identical soaking conditions (Fig. 4a and b).

Visual and FTIR contour maps of an unfilled BTH resin disk after soaking, and of u-, Si-, Zr, Si/Si and Zr/Zr-ACP based BTH composite disk fragments after soaking and BFS testing are presented in Fig. 5a–g. Explanatory color codes for the PO_4 and CO distribution for each specimen were placed between each pair of maps. The colors stand for the area under the PO_4 and CO peaks. Pink represents the lowest area and blue represents the highest area. A predominantly heterogeneous distribution of the mineral PO_4 was noticed on the surfaces of most of the disks regardless of the type of the filler utilized. The Si-ACP/BTH specimen shown presents an extreme case where no PO_4 was found on either surfaces of the disk fragment (PO_4 map, Fig. 5c). Because the XRD of this specimen indicated the presence of ACP in the bulk of the disk's fragment, its cross section (CS) was mapped. The PO_4 map of the CS showed the presence of PO_4 in the center of it (yellow–green–blue colors, Fig. 5d.) A PO_4-rich area was identified at the original, un-fractured edge of a Zr-ACP/BTH disk fragment while the rest of the disk contained much less PO_4 (PO_4 map, Fig. 5e). High PO_4 levels (blue-green regions, PO_4 map, Fig. 5f) are seen in most of the areas of a Si/Si-ACP/BTH disk fragment except in the voids. Much lower concentrations of relatively homogeneously distributed PO_4 (green–yellow–orange spots, PO_4 map, Fig. 5g) were identified on the surface of a Zr/Zr-ACP/BTH disk specimen. In addition, a small spot of impurity, most probably related to zirconium phosphate was seen in the top left edge of that disk (Fig. 5g, blue spot indicated by red arrow in the Zr map). In contrast to the PO_4 maps, CO maps processed within the same color ranges showed quite a homogeneous distribution of the organic matrix of the composites in all specimens. The above described maps are estimated to represent only a 0.1–0.2% of the total sample thickness (FTIR beam penetrates only a few μm of the total specimen thickness (1.5–1.8 mm)). Therefore, they may not be indicative of the overall distribution of the filler throughout the body of the composite specimens. Note the results of the surfaces and the CS of the Si-ACP/BTH specimen (Fig. 5c and d).

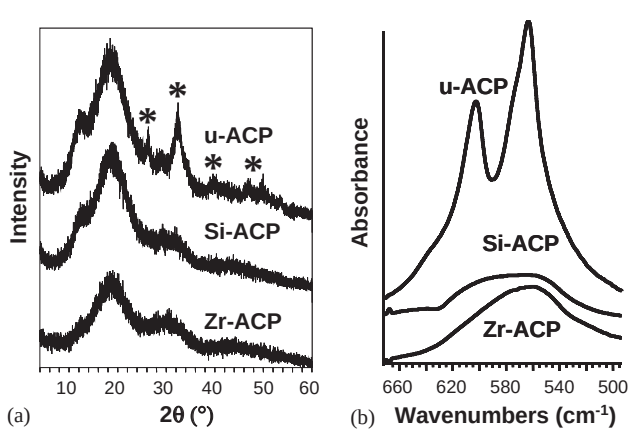

Fig. 4. XRD patterns (a) and the PO_4 bending region (a region with the minimal resin interference) of the corresponding FTIR spectra (b) of u- and hybrid ACP composite disk specimens after 240 h of soaking in buffered saline solutions. The ∗ in (a) represents Ap peaks. The splitting of the u-ACP spectra in (b) also is indicative of conversion to apatite.

Reflectance FTIR spectra are generally different from the corresponding transmission spectra: the bands have a derivative-like shape and the peaks are slightly shifted [9]. The procedure for transforming the reflectance spectra to "absorbance-like" spectra and comparing the "absorbance-like" spectra extracted from the maps with the corrected, reflectance-obtained spectra of standards is illustrated in Fig. 6a–c. Spectra of KBr-embedded synthetic Ap (prepared at 37°C and pH 7.4), u-ACP filler, ground Zr/Zr-ACP/BTH composite and ground polymerized unfilled BTH resin (copolymer) obtained in transmission mode are shown in Fig. 6a. Representative dispersion-corrected spectrum extracted from the maps of Zr/Zr-ACP/BTH composite and BTH copolymer disk specimens in comparison with dispersion-corrected spectra of pressed powders of Ap and u-ACP (same powders that were embedded in KBr, Fig. 6a) acquired in reflectance mode are presented in Fig. 6b. It can be seen that after correcting for dispersion, the shape of the peaks and the location of the CO peak of the resulting "absorbance-like" spectra are quite close to those obtained in transmission. Dispersion-corrected spectra extracted from the maps of the various disk specimens, arranged by the decreasing area of the PO_4 peak are compiled in Fig. 6c. The PO_4 appears as a large shoulder in the resin's ester peak (980–1200 cm^{-1}) in the Zr-, Si/Si- and Zr/Zr-ACP/BTH specimens. The separated PO_4 peak in the spectrum of the u-ACP/BTH composite relates to Ap. The XRD of this specimen showed poorly crystalline Ap, while the patterns of the other specimens in Fig. 5 were of ACP. This accelerated intra-composite ACP to Ap conversion has taken place in all u-ACP/BTH composites. The representative spectrum that was extracted from the Si-ACP/BTH composite disk is identical to the spectrum of the unfilled BTH copolymer (Fig. 6c) indicating that the whole surface of this specimen is PO_4-depleted (as seen in the map in Fig. 5c).

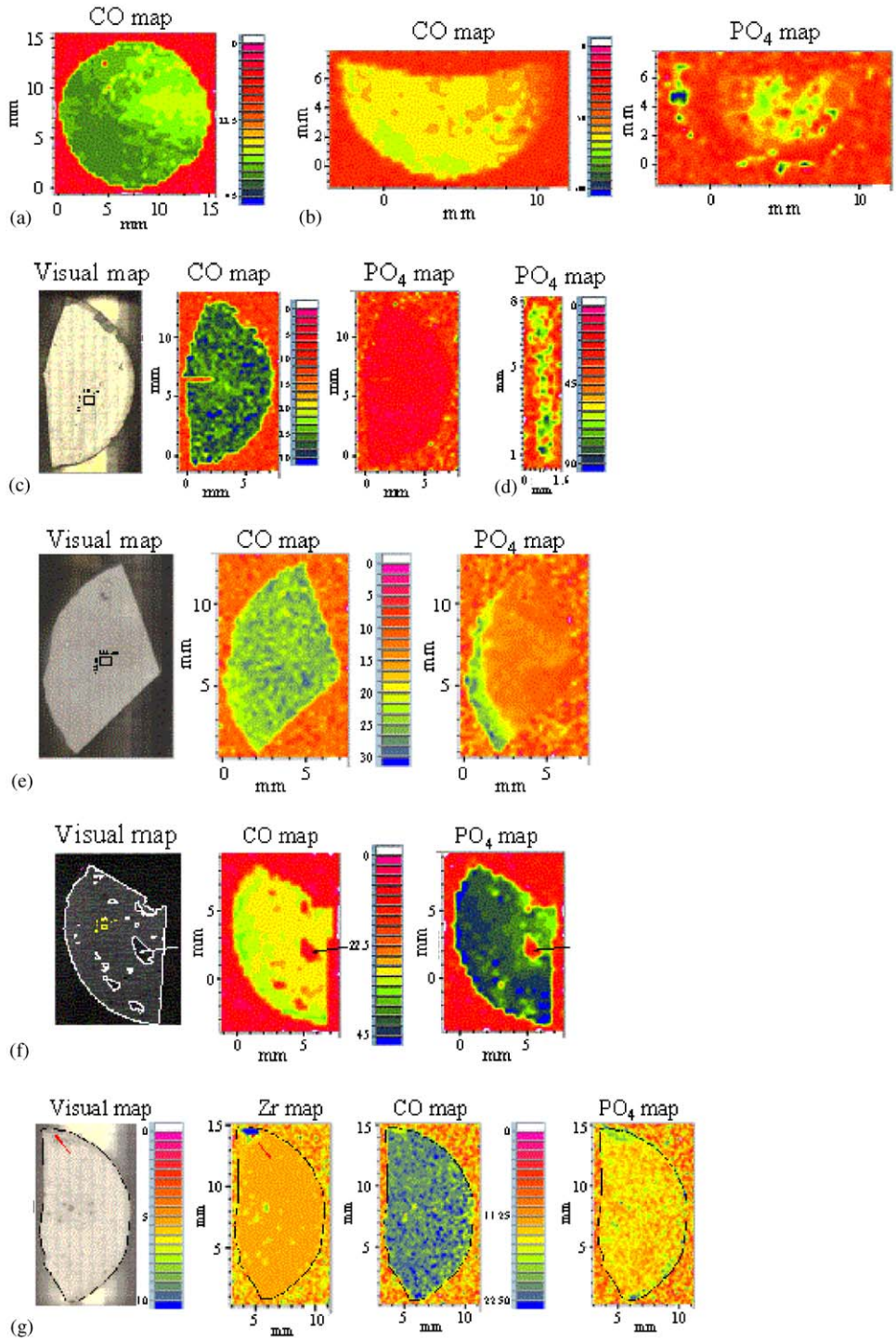

Fig. 5. FTIR microspectroscopic characterization of composite disk specimens: (a) CO map of a whole unfilled BTH disk specimen; (b) CO and PO_4 maps of u-ACP/BTH disk fragment; (c) visual, CO and PO_4 maps of Si-ACP/BTH disk fragment; (d) PO_4 map of the cross section of the Si-ACP/BTH disk fragment shown in (c); (e) and (f) visual, CO and PO_4 maps of Zr-ACP/BTH and Si/Si-ACP/BTH disk fragments, respectively; (g) visual, Zr, CO and PO_4 maps of Zr/Zr-ACP/BTH disk fragment. The colors that represent diminishing areas of the CO and PO_4 peaks are as follows: blue > green > yellow > orange > red.

4. Discussion

Although no detectable differences were found in the structure of hybrid and surface-modified fillers compared to u-ACP, a distinct difference was found in their Ca/PO_4 molar ratios. The Ca/PO_4 molar ratios of Zr-hybridized or surface treated fillers were consistently higher than the Ca/PO_4 molar ratio of u-ACP or Si-ACP and Si/Si-ACP. The reason for the observed difference is seemingly the phosphate uptake due to

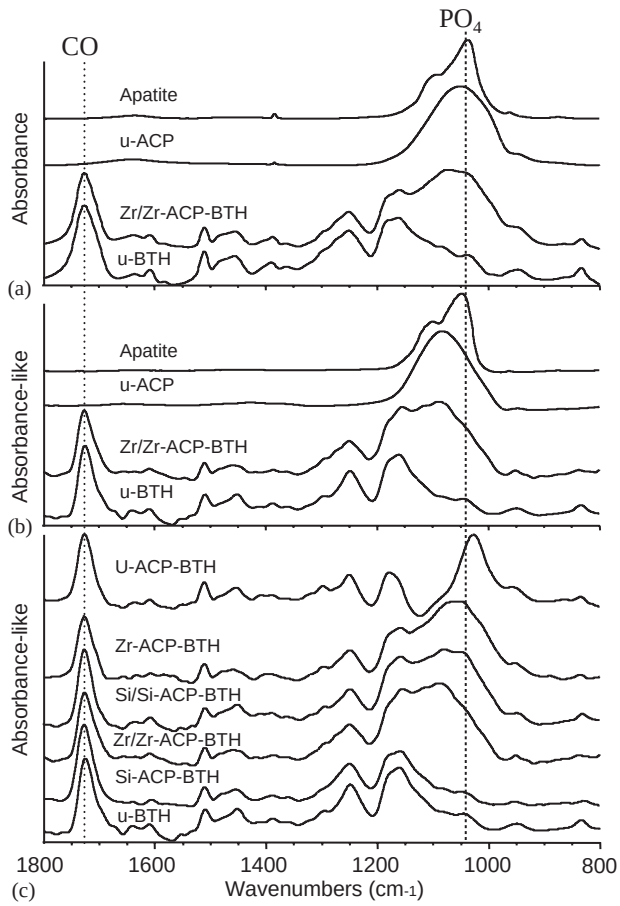

Fig. 6. Absorbance FTIR spectra of synthetic Ap, u-ACP filler, ground Zr/Zr-ACP/BTH composite and ground BTH copolymer embedded in KBr pellets and acquired in transmission mode (a). Dispersion-corrected, absorbance-like spectra of the same specimens acquired in reflectance mode (b). Dispersion-corrected, reflectance FTIR spectra (arranged by the decreasing intensity of the PO_4 peaks) of u-ACP/BTH composite, Zr-ACP/BTH composite, Si/Si-ACP/BTH composite, Zr/Zr-ACP/BTH composite, Si-ACP/BTH composite and the unfilled BTH resin extracted from the maps of the specimens are shown in Fig. 5.

the concomitant formation of HCl-insoluble Zr-PO_4 compounds in the synthesis of Zr-ACP and Zr/Zr-ACP fillers.

SEM examinations did not show any alteration in the morphology of ACP powders upon hybridization and/or surface treatment, nor were there any significant changes in the PSD of ACP following these treatments.

The non-homogeneity in filler distribution seen in the FTIR maps of some of the surfaces of hybridized and/or surface treated ACP composites, after immersion, may have resulted from excessive agglomeration due to anti-dispersive interactions with the resin components during the composites preparation.

FTIR microspectroscopic mapping also revealed that the subsurface voids that appear as cavities/defects in the visual maps were particularly evident in Si/Si-ACP/BTH specimens (Fig. 5e). These defects were less abundant in Zr/Zr-ACP/BTH composite specimens. The FTIR analyses suggest that filler non-homogeneity and the existence of a higher number of defects/voids (originating from the mechanical defects and/or dissolved ACP) throughout the body of composite disk specimens may explain in part why soaking had such deleterious effect on their mechanical strength. Whether they also contributed in some way to the lower release of mineralizing ions remains an open question. Possibly water absorbed preferentially by voids. Nevertheless, non-uniformity of the composite surfaces provides defects for the large calcium and phosphate reservoirs. It is postulated that cracks that form upon soaking of the composites penetrate to reservoirs and serve as the avenues (channels) for the remineralizing Ca^{2+} and PO_4 ions to diffuse out to the external milieu.

Results from this study also showed that resin composition as well as the type of filler used can strongly affect both the mechanical and the ion-release profiles of the composites. Hybridized ACP fillers, for example, produced stronger composites only with BTHZ resins. It will be prudent to explore other resin formulations that include urethane dimethacrylate (UDMA) or ethoxylated bisphenol A dimethacrylate (EBPADMA) as base monomers. UDMA has been shown to reduce water sorption and polymerization shrinkage while enhancing the mechanical properties of resin matrices [17]. Dental polymers based on EBPADMA, a relatively hydrophobic base monomer with more flexible structure and low viscosity, show higher degrees of cure and lower polymerization shrinkages than Bis-GMA/TEGDMA resins [18].

While the agglomeration of Ap has received limited attention [19,20], ACP's agglomeration has not been investigated at all. The process is likely to be of great importance in the formation of both normal and pathological mineral deposits in the human body due to the interaction of proteins and bacteria with crystallites of the mineral phase. As discussed above, agglomeration of ACP fillers can strongly influence filler/resin matrix interactions and, as such, is critical in maintaining the mechanical integrity of the composites. In future studies we will focus on controlling the excessive agglomeration of ACP fillers and their uneven distribution in composites. Modification of surface-treatment protocols, i.e. either complete elimination of washing steps (to prevent loosely bound surface active functionalities to be washed out from the surface of ACP fillers) or utilization of more polar solvents may be one way of addressing this problem. Introduction of co-cations or polymers during the ACP synthesis is seen as another way of improving the dispersion of ACP by lowering the degree of agglomeration, and affecting solubility by reducing the number of active dissolution sites via surface adsorption of additives, and possibly modify ACP's structure/composition due to structural

incorporation. The FTIR-RM, used to characterize composites for the first time in this study, seems to be most valuable in addressing the problems associated with filler agglomeration. Already shown useful in producing functional group maps and showing their distribution on the surface of immersed disk specimens and in the cross section of the Si-ACP/BTH disk, this technique will be extended to compare the distribution of the various constituents before and after immersion, and to examine cross-sectional changes in composite disk specimens after the BFS measurements.

5. Conclusions

This study reveals that both the resin composition and the type of ACP filler strongly affect the mechanical strength and ion-release profiles of the composites. Utilizing silica- or zirconia-hybridized ACP moderately improves the BFS of Bis-GMA/TEGDMA/HEMA/ZrDMA-based composites while maintaining their high anti-demineralizing/remineralizing potential, i.e. releasing adequate levels of calcium and phosphate ions. Controlling the excessive agglomeration of ACP fillers and their uneven distribution throughout the composite is identified as critical factors in maintaining the mechanical integrity of composites and providing sustained remineralizing activity upon exposure to aqueous environments. FTIR microspectroscopic mapping is established as a valuable tool for assessing the distribution of filler particles on the surface as well as throughout the body of the composite.

Acknowledgements

This investigation was supported, in part, by USPHS Research Grant 13169 to the American Dental Association Foundation from the National Institutes of Health—National Institute of Dental and Craniofacial Research and is part of the dental research program conducted by the National Institute of Standards and Technology in cooperation with the American Dental Association Foundation.

Disclaimer. Certain commercial materials and equipment are identified in this work for adequate definition of the experimental procedures. In no instance does such identification imply recommendation or endorsement by the National Institute of Standards and Technology or the American Dental Association Foundation or that the material and the equipment identified is necessarily the best available for the purpose.

References

[1] Antonucci JM, Skrtic D, Eanes ED. Bioactive dental materials based on amorphous calcium phosphate. Polym Prepr 1994;35(2):460–1.
[2] Antonucci JM, Skrtic D, Eanes ED. Remineralizing dental composites based on amorphous calcium phosphate. Polym Prepr 1995;36(1):779–80.
[3] Skrtic D, Hailer AW, Takagi S, Antonucci JM, Eanes ED. Quantitative assessment of the efficacy of amorphous calcium phosphate/methacrylate composites in remineralizing caries-like lesions artificially produced in bovine enamel. J Dent Res 1996;75(9):1679–86.
[4] Skrtic D, Antonucci JM, Eanes ED. Improved properties of amorphous calcium phosphate fillers in remineralizing resin composites. Dent Mater 1996;12:295–301.
[5] Skrtic D, Antonucci JM, Eanes ED, Eichmiller FC, Schumacher GE. Physicochemical evaluation of bioactive polymeric composites based on hybrid amorphous calcium phosphates. J Biomed Mater Res 2000;53:381–91.
[6] Chalmers JM, Everall NJ, Ellison S. Specular reflectance: a convenient tool for polymer characterisation by FTIR-microscopy? Micron 1996;27(5):315–28.
[7] Wentrup Byrne E, Rintoul L, Smith JL, Fredericks PM. Comparison of vibrational spectroscopic techniques for the characterization of human gallstones. Appl Spectroscopy 1995;49(7):1028–36.
[8] Rintoul L, Panayiotou H, Kokot S, George G, Cash G, Frost R, Bui T, Fredericks P. Fourier transform infrared spectrometry: a versatile technique for real world samples. Analyst 1998;123(4): 571–7.
[9] Tesch W, Eidelman N, Roschger P, Goldenberg F, Klaushofer K, Fratzl P. Graded microstructure and mechanical properties of human crown dentin. Calcif Tissue Int 2001;69(3):147–57.
[10] Eanes ED, Gillessen IH, Posner AS. Intermediate states in the precipitation of hydroxyapatite. Nature 1965;208:365–7.
[11] Monte SJ. Ken-React reference manual: titanate, zirconate and aluminate coupling agents. Bayonne: Kenrich Petrochemicals; 1993. p. 1–106.
[12] Murphy J, Riley JP. A modified single solution method for the determination of phosphate in natural waters. Anal Chim Acta 1962;27:31–6.
[13] Kirsten AF, Woley RM. Symmetrical bending of thin circular elastic plates on equally spaced point supports. J Res Natl Bureau Stand 1967;71C:1–10.
[14] Wachtman Jr. JB, Capps W, Mandel J. Biaxial flexure tests of ceramic substrates. J Mater 1972;7:188–94.
[15] Reffner JA, Wihlborg WT. Microanalysis by reflectance FTIR microscopy. Am Lab 1990;22(6):26.
[16] Skrtic D, Antonucci JM, Eanes ED. Effect of the monomer and filler systems on the remineralizing potential of bioactive dental composites based on amorphous calcium phosphate. Polym Adv Technol 2001;12:369–79.
[17] Skrtic D, Antonucci JM, Eanes ED. Amorphous calcium phosphate-based bioactive polymeric composites for mineralized tissue regeneration. J Res Natl Inst Stand Technol 2003;108: 167–82.
[18] Antonucci JM, Liu DW, Stansbury JW. Synthesis of hydrophobic oligomeric monomers for dental applications. J Dent Res 1993; 72:369.
[19] Hansen NM, Felix R, Bisaz S, Fleish H. Aggregation of hydroxyapatite. Bioch Biophys Acta 1976;51:549–59.
[20] Nancollas GH, Budz JA. Analysis of particle size distribution of hydroxyapatite crystallites in the presence of synthetic and natural polymers. J Dent Res 1990;69(10):1678–85.